Author(s): Shen, Hui; Xu, Zhen; Hazer, Maryam Sabooni Asre; Wu, Qingyuan; Peng, Jiang;
Qin, Ruixuan; Malola, Sami; Teo, Boon K.; Häkkinen, Hannu; Zheng, Nanfeng

Title: Surface Coordination of Multiple Ligands Endows N-Heterocyclic Carbene-Stabilized
Gold Nanoclusters with High Robustness and Surface Reactivity

Year: 2021

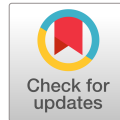Version: Accepted version (Final draft)

Please cite the original version:

Shen, H., Xu, Z., Hazer, M. S. A., Wu, Q., Peng, J., Qin, R., Malola, S., Teo, B. K., Häkkinen, H., &
Zheng, N. (2021). Surface Coordination of Multiple Ligands Endows N-Heterocyclic Carbene-
Stabilized Gold Nanoclusters with High Robustness and Surface Reactivity. Angewandte Chemie,
60(7), 3752-3758. https://doi.org/10.1002/anie.202013718

Check for
updates

Accepted Article

Title: Surface Coordination of Multiple Ligands Endows N-Heterocyclic Carbene-Stabilized Gold Nanoclusters with High Robustness and Surface Reactivity

Authors: Hui Shen, Zhen Xu, Maryam Sabooni Asre Hazer, Qingyuan Wu, Jiang Peng, Ruixuan Qin, Sam Malola, Boon K. Teo, Hannu Häkkinen, and Nanfeng Zheng

WILEY-VCH

RESEARCH ARTICLE

Surface Coordination of Multiple Ligands Endows N-Heterocyclic Carbene-Stabilized Gold Nanoclusters with High Robustness and Surface Reactivity

Hui Shen, Zhen Xu, Maryam Sabooni Asre Hazer, Qingyuan Wu, Jian Peng, Ruixuan Qin, Sami Malola, Boon K. Teo,* Hannu Häkkinen, and Nanfeng Zheng*

[a]   H. Shen, Z. Xu, Q. Y. Wu, Dr. J. Peng, Dr. R. X. Qin, Prof. B. K. Teo, Prof. N. F. Zheng
       State Key Laboratory for Physical Chemistry of Solid Surfaces, Collaborative Innovation Center of Chemistry for Energy Materials, and National & Local
       Joint Engineering Research Center for Preparation Technology of Nanomaterials, College of Chemistry and Chemical Engineering, Xiamen University
       Xiamen 361005, China
       E-mail: nfzheng@xmu.edu.cn
               boonkteo@xmu.edu.cn
[b]   M. Hazer, Dr. S. Malola, Prof. H. Häkkinen
       Departments of Physics and Chemistry, Nanoscience Center, University of Jyväskylä
       FI-40014 Jyväskylä, Finland

       Supporting information for this article is given via a link at the end of the document.

Abstract: Deciphering the molecular pictures of the multi-component and non-periodic organic-inorganic interlayer is a grand technical challenge. Here we show that the atomic arrangement of hybrid surface ligands on metal nanoparticles can be precisely quantified through comprehensive characterization of a novel gold cluster, $Au_{44}(^{i}Pr_2\text{-bimy})_9(PA)_6Br_8$ (**1**), which features three types of ligands, namely, carbene (1,3-diisopropylbenzimidazolin-2-ylidene, $^{i}Pr_2$-bimy), alkynyl (phenylacetylide, PA), and halide (Br), respectively. The delicately balanced stereochemical effects and bonding capabilities of the three ligands give rise to peculiar geometrical and electronic structures. Remarkably, despite its complex and highly distorted surface structure, cluster **1** exhibits unusual catalytic properties and yet it is highly stable, both chemically and thermally. Moreover, rich reactive sites on the cluster surface raise the prospect of bio-compatibility (as it can be functionalized to yield water-soluble derivatives) and bio-applications.

Introduction

The metal-ligand interface of metal nanomaterials is crucial to their overall properties, as their electronic structures, local coordination environments and physicochemical properties are sensitive to its subtle change. [1] During the past decades, great progress has been made in engineering interface of metal nanomaterials via single ligand systems such as phosphine, thiol, alkynyl, halide, and N-heterocyclic carbene (NHC).[2] Recently, hybrid ligands have been used to endow metal nanomaterials with better performance than either of single ligand systems. [3] However, in sharp contrast to the well-studied pure-ligand-metal interface, it remains an unsettled front for today's characterization techniques to fully identify the detailed binding structures in mixed-ligand metal nanomaterial systems, as they often lead to highly complicated surface structures or dynamic ligand arrangements. [4] Atomically precise monolayer-protected metal nanoclusters (NCs) have found many benefits in illustrating the metal-ligand

interface structures. [5] With help from single-crystal X-ray crystallography, surface features of several important ligands on metal nanoparticles have been revealed, in which single or double types of ligands were often used. [6] In the community, NHCs represent a new class of ligands in stabilizing and activating clusters. [7] Examples include Au_{11}, [7a] Au_{13}, [7b, 7c] and Au_{25} [7d] NCs featuring gold-carbene interface have been reported. As part of our continuing effort in the study of metal-carbene interface in metal nanomaterials, it occurred to us that mixed ligands on a metal cluster surface may give rise to novel nanomaterials with unusual properties. The rationale behind this idea is that delicately balanced stereochemical effects and bonding capabilities of multiple types of ligands may create peculiar geometrical arrangements and synergic electronic effects.

Reported herein is the synthesis, structure and catalysis of a novel gold cluster, $Au_{44}(^{i}Pr_2\text{-bimy})_9(PA)_6Br_8$ (**1**), that is surface capped by nine 1,3-diisopropylbenzimidazolin-2-ylidene ($^{i}Pr_2$-bimy), six phenylacetylides (PA), and eight bromides. Three different types of ligands (i.e., N-heterocyclic carbenes, alkynyls, and halides) are present on the surface of the cluster. As a result, it displays unprecedented metal framework and ligand arrangements as well as electronic structure. Furthermore, the diverse surface structures endow the title cluster with different capabilities: the presence of bromides on the cluster allows the surface modification to bio-compatibility; the NHCs give rise to high thermal stability; and the labile alkynyl ligands facilitate the interaction between substrates and active surface sites, leading to excellent performance in catalysis.

Results and Discussion

Synthesis and atomic structure

Based on our previous demonstration on the excellent stability of NHC-stabilized AuNCs that were prepared from direct reduction of NHC-Au-X (X=Cl and Br) precursors, we expected that the introduction of other ligands in the synthesis should help

RESEARCH ARTICLE

to create robust but surface-active Au NCs with reactant-binding sites for promoting catalysis. The title cluster was thus synthesized by the reduction of NHC-AuX (X=Cl and Br) in the presence of phenylacetylene (PA) (see SI for details). In a typical synthesis, equivalent amount of ^{i}Pr$_2$-bimyAuCl and ^{i}Pr$_2$-bimyAuBr was dissolved in mixed solvent of tetrahydrofuran/dichloromethane. A methanol solution of PA with MeONa used for deprotonation was added to the Au precursor solution, followed by the addition of NaBH$_4$ solution to initiate the reduction process. The reaction was kept in stirring continuously for 30 h in the dark. These clusters are then purified (by column chromatography and washing) and crystallized from a toluene/hexane mixture, giving rise to the growth of black crystals after about 4 weeks.
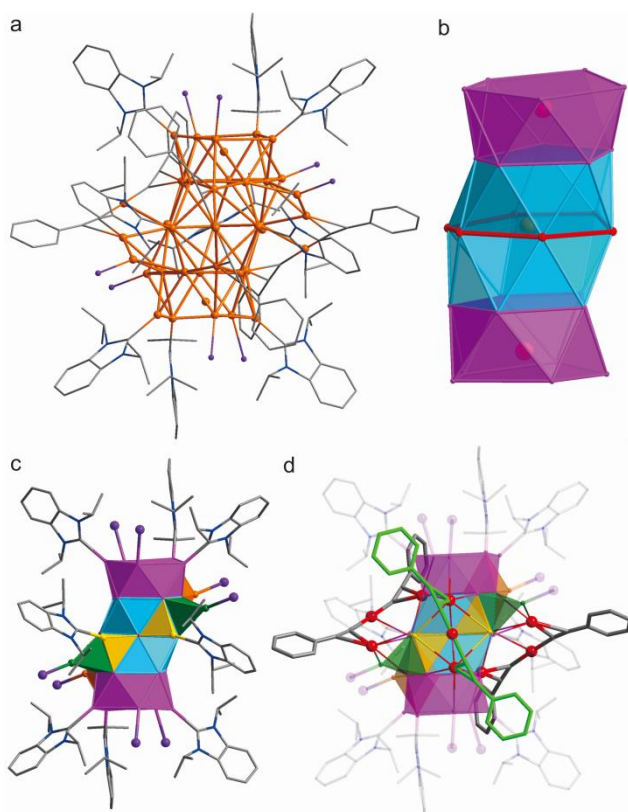

Figure 1. a) Total structure of **1**; b) the Au$_{29}$ core; c) coordination modes of surface NHC and Br ligands; d) binding structures of surface alkynyl ligands in **1**. Color legends: orange, pink, red, green, and yellow, Au; purple, Br; blue, N; gray and bright green, C. H atoms are omitted for clarity.

The structure of **1** was determined by single-crystal X-ray crystallography and characterized as Au$_{44}$(^{i}Pr$_2$-bimy)$_9$(PA)$_6$Br$_8$ (Figure S1). It crystallizes in the monoclinic space group C2/c (Table S1), with four clusters per unit cell (Figure S2). There was no counterion observed in the lattice, indicating it is a neutral molecule. Shown in Figure 1a and Figure S3a is the overall structure of **1** in different views. There is a crystallographic twofold (C2) symmetry axis, passing through four Au atoms (cf. Figure S4 and 5). The metal core of **1** can be described as two pentagonal antiprisms (pink) fused with a peculiar polyhedron consisted of two pentagons and a centered hexagon (red) (Figure 1b and Figure S3b). The encapsulated center Au atom is shown in yellow.

Alternatively, the metal core can be described as a decapped vertex-sharing biicosahedral Au$_{23}$ cluster (cf. Fig. S6), reminiscent of the biicosahedral M$_{23}$ clusters such as [M$_{25}$(PPh$_3$)$_{10}$X$_8$]$^+$ (where M=Au/Ag, X=halides) reported by Teo and coworkers. Here the ring of six halides in the equatorial plane of the latter cluster is replaced by a ring of six capping Au atoms, in addition to the removal of the two metal atoms at the apical positions (Figure S6). [8] As such, the core of **1** is totally different from that of all-alkynyl-stabilized Au$_{44}$ reported by Wang and co-workers (Au$_{34}$ kernel from interpenetrating di-cuboctahedral Au$_{20}$), [9] suggesting the capability of mixed ligands in dictating the cluster structure. The Au$_{29}$ core is capped by six Au atoms, forming triangular prisms and tetrahedrons. The metal framework is further passivated by six PA, nine NHC, and eight Br ligands in multiple coordination environments (Figure 1c and Figure S3c). Nine Au atoms form 3 pairs of Au-PA-Au-PA-Au staple motif, which displays two kinds of binding sites (Figure 1d and Figure S3d). All PA ligands coordinate with Au atoms in μ$_2$-η^1,η^2 mode (Figure 1d). Interestingly, on the surface of **1**, uncoordinated Au atoms are present, providing the feasibility of catalytically activating small molecules (Figure S8). The average Au-Au bond lengths in the decapped centered Au$_{12}$ icosahedron are: Au$_a$-Au$_b$ 2.7716, Au$_b$-Au$_c$ 2.834, Au$_c$-Au$_d$ 3.4516 Å (for subscript labels, see Figure S9). For the Au$_6$ hexagon, the bond distances of Au-Au are averaged to be 2.858 Å. The nine N-heterocyclic carbene ligands coordinate to surface via strong Au-C bonds (2.03 Å, Figure 1c). These Au-C bonds are somewhat stronger than that of [Au$_{25}$(^{i}Pr$_2$-bimy)$_{10}$Br$_7$]$^{2+}$ (2.069 Å), [Au$_{13}$(^{i}Pr$_2$-bimy)$_6$Br$_6$]$^-$ (2.078 Å) and [Au$_{11}$(PPh$_3$)$_7$(^{i}Pr$_2$-bimy)Cl$_2$]Cl (2.09 Å). The eight bromides terminally coordinated to Au atoms with the average Au-Br bond distance of 2.4355 Å (Figure 1c). For detailed arrangements of the ligands, see Fig. S3-9.
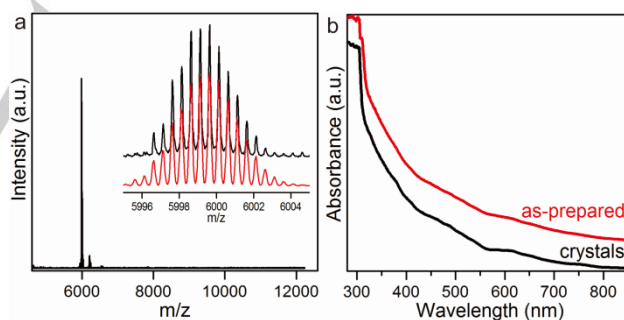

Figure 2. a) HRICR-MS of mixture of **1** and CsOAc in the positive mode. Inset: the comparison of measured (black) and simulated (red) isotopic distribution patterns of [Au$_{44}$(^{i}Pr$_2$-bimy)$_9$(PA)$_6$Br$_8$Cs$_2$]$^{2+}$; b) UV/Vis spectra of as-prepared product and single crystal of **1** in dichloromethane.

The composition of **1** was confirmed by high resolution ion cyclotron resonance mass spectrometry (HRICR-MS). The HRICR-MS spectrum of **1** after mixing with excess CsOAc exhibits a single peak at 5999.6 m/z, corresponding to [Au$_{44}$(^{i}Pr$_2$-bimy)$_9$(PA)$_6$Br$_8$Cs$_2$]$^{2+}$ (Figure 2a). The composition was also supported by proton nuclear magnetic resonance spectroscopy (^{1}H NMR). As shown in Figure S10, all characteristic peaks of **1**, including six alkynyl and nine NHC ligands, can be properly assigned (Table S2), which again proves the purity and composition of the cluster.

2

RESEARCH ARTICLE

Electronic structure and optical properties

Cluster **1** exhibits unique electronic structure, as suggested by its distinct optical absorption spectrum in the UV/Vis region (Figure 2b). We note that UV/Vis spectrum of raw product resembles that of single crystals, suggesting the high purity of the clusters in as-prepared product.

Electronic structure and optical properties of **1**, using the experimental structure directly, were investigated via density functional theory (DFT) calculations (see technical details in the SI). The ground state electronic structure, solved by using the Perdew-Burke-Ernzerhof (PBE) exchange-correlation functional, [10] displays a clear HOMO-LUMO energy gap of 0.64 eV and a series of rather well-defined symmetries of several molecular orbitals around the gap (Figure 3). The clear HOMO-LUMO gap reinforces the experimental indication that cluster **1** is electronically stable as a neutral species. Count of delocalized "superatom" electrons[11] from the chemical formula of **1** yields 30. This number is a non-magic electronic number for spherical systems but stabilizes the energy gap in the strongly non-spherical cluster **1** as seen in Figure 3. Nevertheless, it is instructive to analyze the global symmetries of several frontier orbitals by projecting them to spherical harmonics. The electron count of 30 implies that one resides in the spherical F shell (that spans the symmetries between 20 and 34 electrons occupied in 7 orbitals). Indeed, Figure 3 clearly displays 5 states of F symmetry below HOMO, in addition, LUMO and LUMO+1 also have the F symmetry while several states starting from LUMO+3 display a dominant G symmetry. The HOMO state, interestingly, displays a mixed S-G symmetry and is somewhat reminiscent of the spherical 2S state (see also the visualizations of the frontier orbitals in Figure S14). The strongly non-spherical and low-symmetry atomic structure of **1** is thus seen to severely split degeneracies and distort the spherical symmetries while their remnants are still identifiable.
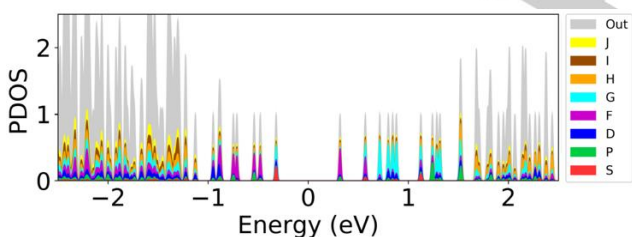

Figure 3. Electronic density of states of **1**, projected onto spherical harmonics. The HOMO-LUMO gap is centered around zero.

The HOMO-LUMO gap of 0.64 eV predicts that the optical absorption should extend well into the near-infrared region. This is indeed the case: both the measured (Figure 2b) and computed (Figure S15) absorption curves display non-zero absorption at least down to 900 nm.

Atomic charges were analyzed by the Bader method and are shown in Table S3. The analysis indicates that the 3 Au atoms bound between the PA ligands in the ligand layer are significantly positively charged (0.25e) while the other 41 Au atoms are essentially neutral. Br and PA ligands have negative charge (-0.45e and -0.29e, respectively) as expected for their electron-withdrawing nature. NHC ligands show positive charge (0.35e) as

expected for a weak electron donor. This analysis indicates that the multiple-ligand interface found in cluster **1** has a rich variation of local charges, which may be important for its surface reactivity (see below).

Stability and surface reactivity

With NHCs as the stabilizing ligands, **1** exhibits a high physical stability. Its UV/Vis profile was practically unchanged upon heating at 65 °C in the solution form for 12 h (Figure 4a), consistent with the observation in other NHC-stabilized Au NCs. Such a high stability is important to many of their applications, in particular to demonstrating the structure-properties relationship. Bearing halides on surface, **1** can be easily converted into a water-soluble product via ligand exchange. It can be readily transferred into aqueous phase upon adding aqueous mercaptosuccinic acid into toluene solution of **1** (Figure 4b). The aqueous solution of the obtained products exhibited practically the same UV/Vis spectrum, indicating that the metal core remained intact after the ligand exchange (Figure S16a). As revealed by the electrospray ionization mass spectrometric (ESI MS) measurement (Figure S16b), a maximal value of 8 bromides of **1** were exchanged by thiolates, thereby creating new functionalities for potential applications requiring good water solubility. [12] It should be noted that to avoid the ligand exchange with different types of ligands on surface, the molar ratio of mercaptosuccinic acid to the cluster used in this work was 10, which might also help to explain the exchange at Br⁻ sites only. However, the relatively low weak ESI-MS signal with limited resolution does not allow us to exclude the other ligand exchanging possibility.
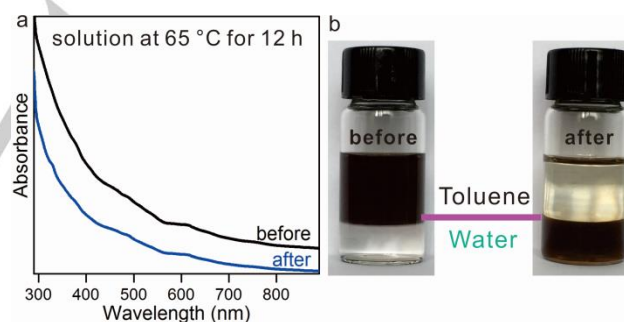

Figure 4. a) UV/Vis spectral study of cluster **1** before and after 12 h of heating in 1,2-dichloroethane at 65 °C; b) photographs of the solution of **1** before and after ligand-exchange with mercaptosuccinic acid, followed by dissolving in a mixture of toluene and water.

Catalytic performance

In a catalytic reaction, reactants are typically bound on the catalyst's surface and thus activated for the subsequently chemical transformation. To act as an effective catalyst, metal clusters should possess binding sites for the activation of reactants. The following structure features of **1** makes it a good cluster catalyst candidate: (1) the excellent stability enhanced by the NHC ligands; (2) the presence of surface Au(I) sites for binding alkynyl groups; (3) the remaining metal open sites that are adjacent to the alkynyl binding sites. To test these hypotheses,

3

RESEARCH ARTICLE

we evaluated the so-called solvent-accessible surface area (SASA) for small molecules in contact with gold atoms in the cluster (see details in SI text). As shown in Figure 5 and Figure S17-18. The identified large areas of accessibility are at top of those Au(I) sites in the three PA-Au(I)-PA surface units while the secondary small accessible areas (highlighted by red arrows) are also available at the top of surface uncoordinated Au sites that are adjacent to Au(I) sites. The largest solvent-accessible "pockets" can accommodate bigger molecules of up to about 6.2 Å steric radius, which may facilitate co-binding and simultaneous interaction of two reactant molecules (Figure S18).
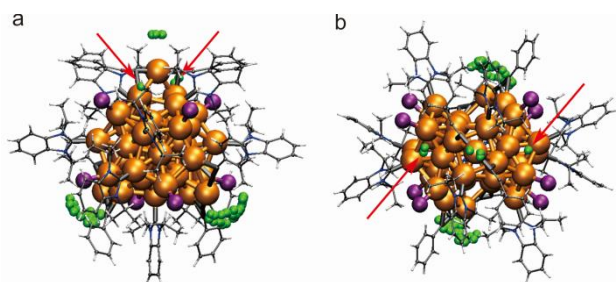

Figure 5. Visualization of the SASA of cluster **1**. The green small spheres denote potential centers of water molecules (modelled by spheres with a radius of 1.4 Å) when they are in contact with Au atoms in the cluster. The cluster is viewed from two different directions (a and b) for better visualization.
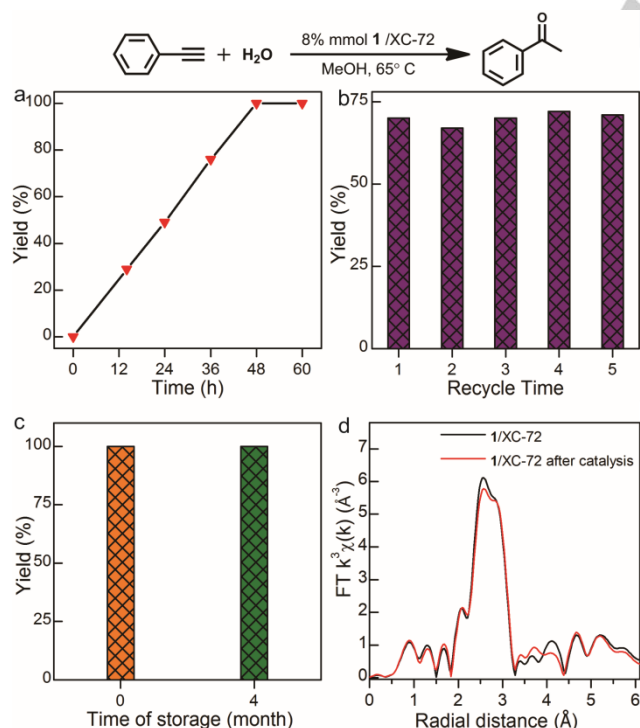
As an example, the hydration of alkynes was chosen for the catalysis evaluation, as it is a straightforward and atom-economical method to prepare carbonyl compounds. [13] To facilitate the separation and recycling of the catalyst, cluster **1** was supported on commercially available activated carbon (XC-72). The catalytic reaction was conducted by adding 8% mmol (based on Au) of **1**/XC-72 to a solution of PA and H_2O in organic solvents (see SI for details). The catalyst succeeded in accelerating the hydration of PA to acetophenone at 65 °C (cf. Table S4, entry 1). The catalytic conditions were optimized by exploring the solvent effects. It was found that the reaction worked well in methanol, ethylene glycol, and 1, 2-dichloroethane (Table S4, entry 2-5), but inactive in N,N-dimethylformamide. As illustrated in Figure 6a, the cluster displayed an extremely high activity in the first run as its conversion close to 100% after 48 h. Also, the catalyst is highly stable, yielding a constant reaction rate during the catalytic cycles (up to 550 turnovers and beyond). No detectable decay in the catalytic activity during the whole catalytic process was observed. We note that besides aforementioned SASA evaluation (Figure 5 and Figure S17-18), the importance of metal open sites could also be verified experimentally, as the catalyst exhibits no activity in N,N-dimethylformamide (Table S4, entry 3), and activity of the catalyst decreased significantly after being treated with CO (Figure S19), in which either N,N-dimethylformamide or CO would strongly bind with the open sites and thus poison the catalyst. [14]

Figure 6. Catalytic properties of **1**. a) Catalytic performances of 8% mmol **1**/XC-72 (based on Au) recorded at different reaction time points for the hydration of phenylacetylene in the first run; b) recyclability of XC-72 supported **1** in term of activity (36 h); c) Long-term durability of **1**/XC-72 in hydration of phenylacetylene (yield was determined on 48 h catalysis). The catalyst was stored in air in the dark for 4 months. d) Comparison of EXAFS spectra for freshly prepared **1**/XC-72 (black) and post-catalysis **1**/XC-72 (red). Reaction conditions: PA (0.25 mmol), H_2O (7 mmol), CH_3SO_3H (81 uL), 8% mmol catalyst (based on Au), N_2 atmosphere, methanol as solvent, 65 °C, 1, 3, 5-trimethoxybenzene as internal standard, yield was determined by ^1H NMR.

Table 1. A comparison of catalytic activity of different catalysts

Entry	Catalyst[a]	Time (h)	Yield (%)[b]
1	Au_{44}/XC-72	48	>99
2	XC-72	48	trace
3	Au_{44}/TiO_2	48	95
4[c]	$^iPr_2$-bimyAuCl	48	22
5[c]	$^iPr_2$-bimyAuBr	48	26
6	$Au_{25}(SR)_{18}$/XC-72	48	26
7	$Au_{23}(PA)_9(PPh_3)_6$/XC-72	48	29
8	$Au_{25}(^iPr_2$-bimy$)_{10}Br_7$/XC-72	48	18
9[d]	$Au_{13}(NHC)_5Br_2$/XC-72	48	28
10	Au NPs/ TiO_2	48	32

[a] Reaction conditions: PA (0.25 mmol), H_2O (7 mmol), CH_3SO_3H (81 uL), 8% mmol catalyst (based on Au), N_2 atmosphere, methanol as solvent, 65 °C. [b] Measured by ^1H NMR using 1, 3, 5-trimethoxybenzene as internal standard. [c] XC-72 was added together with the catalyst to keep the same catalysis conditions expect the use of different catalysts. [d] NHC = 1,3-Bis(1-benzyl-1H-benzimidazol-1-ium-3-yl)propane.

As expected by the excellent stability of the cluster, the catalyst displayed excellent recyclability as multiple runs of the reaction afforded the desired product with almost the same reactivity (Figure 6b). Notably, the catalyst is highly robust as it gives rise to nearly identical activity after being stored for more than 4 months (Figure 6c). Under the same condition, some representative Au NCs with other interfaces[15], complexes and nanoparticles, however, exhibit much lower activity, verifying high

RESEARCH ARTICLE

surface reactivity of **1** (Table 1). TEM images (Figure S20) of the spent catalysts demonstrate that the cluster undergoes no size change during the reaction, confirming the robustness of the cluster catalyst against aggregation. Furthermore, X-ray absorption near edge structure (XANES) study reveals that the catalysts experience no decomposition over the process, as suggested by the preservation of metallic state after the catalysis (Figure S21). More accurate analysis from extended X-ray absorption fine structure (EXAFS) R-space spectra[16] revealed that the peaks of the Au-Au and Au-Br bonding paths exhibit nearly the same profiles over the reaction. The corresponding bond lengths and coordination number also showed similar values, clearly implying that the structure of the cluster remained intact during the catalytic process (Figure 6d, S22 and Table S5).
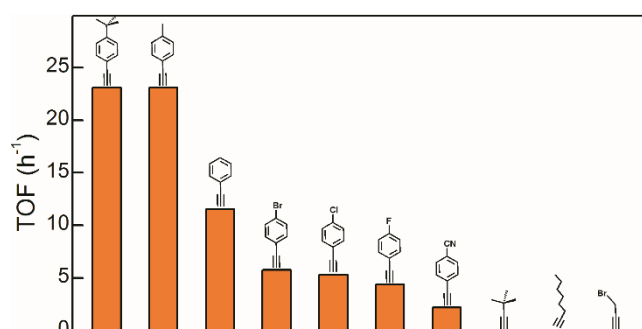

Figure 7. The turnover frequency (TOF) of **1** toward different alkynes, showing its orderly activity for different substrates. Reaction conditions: PA or other alkynes (0.25 mmol), H_2O (7 mmol), CH_3SO_3H (81 uL), 8% mmol catalyst (based on Au), N_2 atmosphere, methanol as solvent, 65 °C, 1, 3, 5-trimethoxybenzene as internal standard, yield was determined by ^1H NMR.

To our surprise, we found the catalyst displays orderly reactivity toward different substrates. For example, it is highly efficient in hydration of aromatic alkynes, especially those bearing electron-donating groups, while practically inactive towards aliphatic alkynes (Figure 7). The situation has not yet been observed in other Au catalysts, indicating the unique catalytic pathways of atomically precise metal NCs. [17] To better understand this interesting difference in catalytic activities toward aromatic vs aliphatic alkynes, we mixed aromatic alkynes (for example, 4-fluorophenylacetylene) or aliphatic alkynes (for example, 3,3-dimethyl-1-butyne) with **1**/XC-72 (see SI for details), respectively. It was observed from ^1H NMR that when 4-fluorophenylacetylene was used, PA was successfully exchanged out of cluster **1**; while for 3,3-dimethyl-1-butyne, no free PA was detected under the same reaction conditions. To gain insight into the reaction mechanism, we have conducted an experiment in which stoichiometric catalyst (based on alkynes) was used in hydration of 4-fluorophenylacetylene. As tracked by ^1H NMR (Figure S25), while only 4-fluorophenylacetylene was present in the solution at 0 min, the appearance of PA ligands exchanged from the parental catalyst was clearly observed in the solution after 10 min. But it should be noted that no product was formed at this initial period although both products of (acetophenone and 4-fluoroacetophenone) were formed at 4 h. These data demonstrate that ligand exchange between foreign 4-fluorophenylacetylene and surface PA proceeded much faster than the hydration step. The catalytic reaction should take place only after alkynes are bound onto the surface of the clusters via ligand exchange. No

hydration activity observed for aliphatic alkynes can be explained by the fact that they cannot be exchanged onto the surface of **1.**

Conclusion

In conclusion, metal NCs featuring mixed ligands are promising strategies in producing novel nanostructures with unusual properties. As exemplified by the title cluster $Au_{44}(^iPr_2$-bimy$)_9(PA)_6Br_8$, three types of ligands, namely, carbene, alkynyl, and halide, are incorporated into a single cluster to give rise to peculiar geometrical and electronic structures of metal clusters. While halides are easily ligand-exchanged by thiols for preparing water soluble cluster, the metal sites coordinated by alkynyls provide potential binding sites for alkyne reactants via ligand exchange. More importantly, the presence of highly bulky carbene ligands helps to create uncoordinated surface metal sites for the binding of H_2O (the second reactant) to achieve the enhanced catalysis in the hydration of alkynes that can be ligand-exchanged onto the cluster. Further work, including preparing NHC-stabilized metal clusters in combination with other ligands, is ongoing with the hope of gaining deeper insights with regards to the catalytic reaction mechanisms.

Acknowledgements

**Keywords:** Cluster compounds • carbene ligands • nanostructures • surface reactivities • catalysis

[1]   a) P. X. Liu, R. X. Qin, G. Fu, N. F. Zheng, *J. Am. Chem. Soc.* **2017**, *139*, 2122-2131; b) Y. Yin, A. P. Alivisatos, *Nature* **2005**, *437*, 664-670; c) Z. Jiang, W. Sun, H. Shang, W. Chen, T. Sun, H. Li, J. Dong, J. Zhou, Z. Li, Y. Wang, R. Cao, R. Sarangi, Z. Yang, D. Wang, J. Zhang, Y. Li, *Energ. Environ. Sci.* **2019**, *12*, 3508-3514.

[2]   a) A. D. Jewell, H. L. Tierney, E. C. H. Sykes, *Phys. Rev. B* **2010**, *82*, 205401 ; b) H. Al-Johani, E. Abou-Hamad, A. Jedidi, C. M. Widdifield, J. Viger-Gravel, S. S. Sangaru, D. Gajan, D. H. Anjum, S. Ould-Chikh, M. N. Hedhili, A. Gurinov, M. J. Kelly, M. El Eter, L. Cavallo, L. Emsley, J. M. Basset, *Nat. Chem.* **2017**, *9*, 890-895; c) C. Vericat, M. E. Vela, G. Benitez, P. Carro, R. C. Salvarezza, *Chem. Soc. Rev.* **2010**, *39*, 1805-1834; d) C. M. Crudden, J. H. Horton, Ebralidze, II, O. V. Zenkina, A. B. McLean, B. Drevniok, Z. She, H. B. Kraatz, N. J. Mosey, T. Seki, E. C. Keske, J. D. Leake, A. Rousina-Webb, G. Wu, *Nat. Chem.* **2014**, *6*, 409-414; e) A. V. Zhukhovitskiy, M. G. Mavros, T. Van Voorhis, J. A. Johnson, *J. Am. Chem. Soc.* **2013**, *135*, 7418-7421; f) J. B. Ernst, C. Schwermann, G. I. Yokota, M. Tada, S. Muratsugu, N. L. Doltsinis, F. Glorius, *J. Am. Chem. Soc.* **2017**, *139*, 9144-9147; g) P. Maity, S. Takano, S. Yamazoe, T. Wakabayashi, T. Tsukuda, *J. Am. Chem. Soc.* **2013**, *135*, 9450-9457.

[3]   a) Y. Yang, H. Qin, M. Jiang, L. Lin, T. Fu, X. Dai, Z. Zhang, Y. Niu, H. Cao, Y. Jin, F. Zhao, X. Peng, *Nano. Lett.* **2016**, *16*, 2133-2138; b) Y. Yang, H. Qin, X. Peng, *Nano. Lett.* **2016**, *16*, 2127-2132.

5

[4]   Z. Pang, J. Zhang, W. Cao, X. Kong, X. Peng, *Nat. Commun.* **2019**, *10*, 2454.

[5]   a) R. Jin, C. Zeng, M. Zhou, Y. Chen, *Chem. Rev.* **2016**, *116*, 10346-10413; b) J. Z. Yan, B. K. Teo, N. F. Zheng, *Acc. Chem. Res.* **2018**, *51*, 3084-3093; c) Z. Lei, X. K. Wan, S. F. Yuan, Z. J. Guan, Q. M. Wang, *Acc. Chem. Res.* **2018**, *51*, 2465-2474; d) Y. Du, H. Sheng, D. Astruc, M. Zhu, *Chem. Rev.* **2020**, *120*, 526-622.

[6]   a) L. C. McKenzie, T. O. Zaikova, J. E. Hutchison, *J. Am. Chem. Soc.* **2014**, *136*, 13426-13435; b) P. D. Jadzinsky, G. Calero, C. J. Ackerson, D. A. Bushnell, R. D. Kornberg, *Science* **2007**, *318*, 430-433; c) M. Zhu, C. M. Aikens, F. J. Hollander, G. C. Schatz, R. Jin, *J. Am. Chem. Soc.* **2008**, *130*, 5883-5885; d) A. Desireddy, B. E. Conn, J. Guo, B. Yoon, R. N. Barnett, B. M. Monahan, K. Kirschbaum, W. P. Griffith, R. L. Whetten, U. Landman, T. P. Bigioni, *Nature* **2013**, *501*, 399-402; e) H. Yang, Y. Wang, H. Huang, L. Gell, L. Lehtovaara, S. Malola, H. Hakkinen, N. F. Zheng, *Nat. Commun.* **2013**, *4*, 2422; f) M. Sugiuchi, Y. Shichibu, K. Konishi, *Angew. Chem. Int. Ed.* **2018**, *57*, 7855-7859; g) X. K. Wan, Q. Tang, S. F. Yuan, D. E. Jiang, Q. M. Wang, *J. Am. Chem. Soc.* **2015**, *137*, 652-655; h) Z. Gan, Y. Lin, L. Luo, G. Han, W. Liu, Z. Liu, C. Yao, L. Weng, L. Liao, J. Chen, X. Liu, Y. Luo, C. Wang, S. Wei, Z. Wu, *Angew. Chem. Int. Ed.* **2016**, *55*, 11567-11571; i) S. S. Zhang, F. Alkan, H. F. Su, C. M. Aikens, C. H. Tung, D. Sun, *J. Am. Chem. Soc.* **2019**, *141*, 4460-4467; j) R. S. Dhayal, J. H. Liao, S. Kahlal, X. Wang, Y. C. Liu, M. H. Chiang, W. E. van Zyl, J. Y. Saillard, C. W. Liu, *Chem. Eur. J.* **2015**, *21*, 8369-8374; k) T. Chen, V. Fung, Q. Yao, Z. Luo, D. E. Jiang, J. Xie, *J. Am. Chem. Soc.* **2018**, *140*, 11370-11377; l) M. J. Alhilaly, M. S. Bootharaju, C. P. Joshi, T. M. Besong, A. H. Emwas, R. Juarez-Mosqueda, S. Kaappa, S. Malola, K. Adil, A. Shkurenko, H. Hakkinen, M. Eddaoudi, O. M. Bakr, *J. Am. Chem. Soc.* **2016**, *138*, 14727-14732; m) W. Du, S. Jin, L. Xiong, M. Chen, J. Zhang, X. Zou, Y. Pei, S. Wang, M. Zhu, *J. Am. Chem. Soc.* **2017**, *139*, 1618-1624; n) M. Qu, H. Li, L. H. Xie, S. T. Yan, J. R. Li, J. H. Wang, C. Y. Wei, Y. W. Wu, X. M. Zhang, *J. Am. Chem. Soc.* **2017**, *139*, 12346-12349; o) H. Shen, E. Selenius, P. Ruan, X. Li, P. Yuan, O. Lopez-Estrada, S. Malola, S. Lin, B. K. Teo, H. Hakkinen, N. F. Zheng, *Chem. Eur. J.* **2020**, *26*, 8465-8470; p) H. Shen, T. Mizuta, *Chem. Asian. J.* **2017**, *12*, 2904-2907; q) S. F. Yuan, C. Q. Xu, J. Li, Q. M. Wang, *Angew. Chem. Int. Ed.* **2019**, *58*, 5906-5909; r) F. Hu, J. J. Li, Z. J. Guan, S. F. Yuan, Q. M. Wang, *Angew. Chem. Int. Ed.* **2020**, *59*, 5312-5315; s) J. Chai, S. Yang, Y. Lv, H. Chong, H. Yu, M. Zhu, *Angew. Chem. Int. Ed.* **2019**, *58*, 15671-15674.

[7]   a) M. R. Narouz, K. M. Osten, P. J. Unsworth, R. W. Y. Man, K. Salorinne, S. Takano, R. Tomihara, S. Kaappa, S. Malola, C. T. Dinh, J. D. Padmos, K. Ayoo, P. J. Garrett, M. Nambo, J. H. Horton, E. H. Sargent, H. Hakkinen, T. Tsukuda, C. M. Crudden, *Nat. Chem.* **2019**, *11*, 419-425; b) M. R. Narouz, S. Takano, P. A. Lummis, T. I. Levchenko, A. Nazemi, S. Kaappa, S. Malola, G. Yousefalizadeh, L. A. Calhoun, K. G. Stamplecoskie, H. Hakkinen, T. Tsukuda, C. M. Crudden, *J. Am. Chem. Soc.* **2019**, *141*, 14997-15002; c) H. Shen, S. Xiang, Z. Xu, C. Liu, X. Li, C. Sun, S. C. Lin, B. K. Teo, N. F. Zheng, *Nano Res.* **2020**, *13*, 1908-1911; d) H. Shen, G. C. Deng, S. Kaappa, T. D. Tan, Y. Z. Han, S. Malola, S. C. Lin, B. K. Teo, H. Hakkinen, N. F. Zheng, *Angew. Chem. Int. Ed.* **2019**, *58*, 17731-17735.

[8]   B. K. Teo, H. Zhang, *Angew. Chem. Int. Ed.* **1992**, *31*, 445-447.

[9]   X. K. Wan, Z. J. Guan, Q. M. Wang, *Angew. Chem. Int. Ed.* **2017**, *56*, 11494-11497.

[10]   J. P. Perdew, K. Burke, M. Ernzerhof, *Phys. Rev. Lett.* **1996**, *77*, 3865-3868.

[11]   M. Walter, J. Akola, O. Lopez-Acevedo, P. D. Jadzinsky, G. Calero, C. J. Ackerson, R. L. Whetten, H. Grönbeck, H. Häkkinen, *Proc. Natl. Acad. Sci. U.S.A.* **2008**, *105*, 9157-9162.

[12]   a) L. T. Ren, P. Yuan, H. F. Su, S. Malola, S. C. Lin, Z. C. Tang, B. K. Teo, H. Hakkinen, L. S. Zheng, N. F. Zheng, *J. Am. Chem. Soc.* **2017**, *139*, 13288-13291; b) Y. Wang, H. F. Su, C. Xu, G. Li, L. Gell, S. C. Lin, Z. C. Tang, H. Hakkinen, N. F. Zheng, *J. Am. Chem. Soc.* **2015**, *137*, 4324-4327.

[13]   J. Oliver-Meseguer, A. Leyva-Perez, S. I. Al-Resayes, A. Corma, *Chem. Commun.* **2013**, *49*, 7782-7784.

[14]   a) M. M. Heravi, M. Ghavidel, L. Mohammadkhani, *RSC Adv.* **2018**, *8*, 27832-27862; b) T. R. Reina, S. Ivanova, M. A. Centeno, J. A. Odriozola, *Front. Chem.* **2013**, *1*, 12; c) C. H. Lin, X. Liu, S. H. Wu, K. H. Liu, C. Y. Mou, *J. Phys. Chem. Lett.* **2011**, *2*, 2984-2988; d) S. Wang, Q. Zhao, H. Wei, J. Q. Wang, M. Cho, H. S. Cho, O. Terasaki, Y. Wan, *J. Am. Chem. Soc.* **2013**, *135*, 11849-11860; e) C. E. Stere, J. A. Anderson, S. Chansai, J. J. Delgado, A. Goguet, W. G. Graham, C. Hardacre, S. F. R. Taylor, X. Tu, Z. Wang, H. Yang, *Angew. Chem. Int. Ed.* **2017**, *56*, 5579-5583; f) K. K. Datta, B. V. Reddy, K. Ariga, A. Vinu, *Angew. Chem. Int. Ed.* **2010**, *49*, 5961-5965.

[15]   X. K. Wan, S. F. Yuana, Q. Tang, D. E. Jiang, Q. M. Wang, *Angew. Chem. Int. Ed.* **2015**, *54*, 5977-5980.

[16]   a) J. Bao, L. Yang, T. Huang, Z. Sun, T. Yao, Y. Jiang, S. Wei, *Radiat. Phys. Chem.* **2017**, *137*, 99-103; b) M. A. MacDonald, D. M. Chevrier, P. Zhang, H. Qian, R. Jin, *J. Phys. Chem. C* **2011**, *115*, 15282-15287; c) A. W. Cook, Z. R. Jones, G. Wu, S. L. Scott, T. W. Hayton, *J. Am. Chem. Soc.* **2018**, *140*, 394-400; d) X. Cai, W. Hu, S. Xu, D. Yang, M. Chen, M. Shu, R. Si, W. Ding, Y. Zhu, *J. Am. Chem. Soc.* **2020**, *142*, 4141-4153.

[17]   a) J. Cordon, G. Jimenez-Oses, J. M. Lopez-de-Luzuriaga, M. Monge, *Nat. Commun.* **2017**, *8*, 1657; b) R. E. Ebule, D. Malhotra, G. B. Hammond, B. Xu, *Adv. Synth. Catal.* **2016**, *358*, 1478-1481; c) S. Liang, J. Jasinski, G. B. Hammond, B. Xu, *Org. Lett.* **2015**, *17*, 162-165.

6

RESEARCH ARTICLE

Entry for the Table of Contents
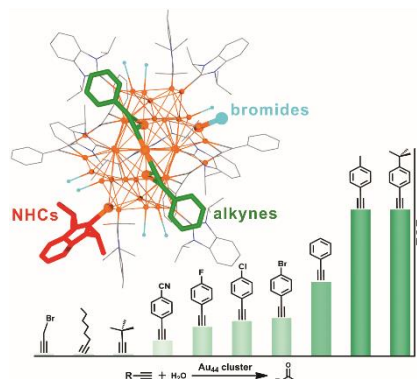
Three metal-ligand interfaces (gold-carbene, gold-alkynyl, and gold-halide) render geometrical, electronic and surface structure of a novel Au_{44} cluster distinct. Due to the hybrid-interface, the cluster exhibits physical, biological and chemical compatibilities. Unprecedentedly, this atomically precise cluster displays orderly reactivity toward different substrates in catalytic hydration of alkynes.